Catalytic Porphyrin Framework Compounds

Liang Feng[1,3,@], Kun-Yu Wang[1,3], Elizabeth Joseph[1] and Hong-Cai Zhou[1,2*]

[1] Department of Chemistry, Texas A&M University, College Station, Texas 77843-3255, United States

[2] Department of Materials Science and Engineering, Texas A&M University, College Station, Texas 77843-3003, United States

[3] These authors contributed equally to this work.

*Correspondence: zhou@chem.tamu.edu

@Twitter: @LiangFe19759953 (L. Feng).

Abstract

Porphyrins are frequently observed in nature and play a vital role in many biological functions, including light-harvesting, oxygen transport, and catalytic transformations. The rigid, robust, and multifunctional features of porphyrins enable the construction of framework compounds such as metal-organic frameworks (MOFs) and covalent organic frameworks (COFs) for use in several important applications. This short review summarizes the types of porphyrin building blocks with varying connectivity, their assembly into framework compounds, and key structural factors governing porphyrin ligand design. Furthermore, we highlight emerging catalytic applications of these porphyrin framework compounds as Lewis acid catalysts, oxidation catalysts, photocatalysts, and electrocatalysts. Together, this review supplies a timely update on porphyrin ligand design and framework compound synthesis, and guides the future development of porphyrin framework compounds with diverse functionalities for efficient catalysis.

Keywords: metal-organic frameworks; covalent-organic frameworks; synthesis; porphyrin; structures; heterogeneous catalysis

Porphyrin Framework Compounds

Porphyrins are a series of substituted porphine compounds that contain heterocyclic macrocycles [1-3]. The name porphyrin originates from the purple coloration that results from light adsorption of the large porphyrin conjugated system in the visible region of the light spectrum. Porphyrin related compounds are commonly observed in nature, and function as essential catalysts for various processes [4, 5]. For example, a porphyrin derivative, heme, can act as a cofactor of hemoglobin in red blood cells to transport oxygen. Another derivative, chlorophyll, which can be found in green plants, is vital for photosynthesis due to its ability to convert sunlight into energy [6].

In addition to their various functions in biochemical, enzymatic, and photochemical processes, the control over rigidity and connectivity of porphyrin **building blocks** (see Glossary) permits their ordered arrangement in crystalline framework materials including **metal-organic frameworks** (**MOFs**) and **covalent organic frameworks** (**COFs**) [7, 8]. Over the last decade, major developments towards precise control over the synthesis of porphyrin-based framework compounds have been observed, allowing the tailoring of their catalytic performance for specific applications [9-11]. Porphyrin framework compounds have become one of the most extensively studied classes of porous materials, often exhibiting the most diverse varieties and functionalities. The facile synthesis, high chemical stability, and robust nature of these compounds has made them an appealing platform for various catalytic applications, including Lewis acid catalysis, oxidation catalysis, photocatalysis, and electrocatalysis [12, 13].

Synthesis and Structural Description of Porphyrin MOFs

MOFs, a well-established class of framework compounds, contain nanoscale pores that can be utilized for recognition, storage, and conversion [14-17]. The modular nature of MOFs permits researchers to design topologies, adjust porosities, and tune functionalities within a single framework by selecting suitable inorganic and organic building blocks [18, 19]. These framework compounds are an excellent platform for aligning and assigning porphyrin functional groups at specific distances for applications such as cooperative catalysis (Figure 1, Table 1).

Porphyrin linkers can serve as building blocks for MOFs owing to their rigid backbones and ease of modification. Through elaborate design of linker connectivity and geometry, the combination of porphyrin linkers with different metal clusters can lead to MOFs with various topologies and functionalities. The connectivity of porphyrin linkers can be tuned from 2 to 8, while the size of the linker can be elongated by incorporating longer arms on the tetrapyrrole ring, allowing for a diverse range of linkers.

The porphyrin linker with the lowest connectivity is 5,15-di(p-benzoato)-porphyrin (DBP, Figure 2). Due to its geometric similarity to the linear linker benzene-1,4-dicarboxylic acid (BDC), DBP is utilized in the construction of **isostructures** of some ubiquitous MOFs.

For instance, in 2016 the Ma group reported MMPF-18 with a **pcu topology**, which was an extended version of MOF-5 [20]. Owing to the *π*-*π* stacking and length of DBP, MMPF-18 featured 4-fold interpenetration. In addition, Lin and coworkers synthesized a series of **hcp** MOFs with M_{12} (M = Zr or Hf) clusters and the DBP linker [21, 22]. The M_{12} cluster was formed by fusing two $Zr_6O_4(\mu_3\text{-}OH)_4$ clusters. The MOF featured an ABBA stacking sequence along the c-axis, instead of an ABC sequence of UiO-type MOFs.

Tetrakis(4-carboxyphenyl)-porphyrin (TCPP), a D_{4h}-symmetric tetratopic linker, has been widely utilized in MOF synthesis. The square geometry of TCPP is rigid, while rotation of the terminal phenyl ring is free. Therefore, diverse metal clusters can be combined with TCPP to afford MOFs with various topologies. For instance, when TCPP is connected to Cu_2 paddlewheel clusters with C_4 symmetry, a **sql** MOF nanofilm NAFS-1 forms [23], and the Cu is replaceable by other metals such as Ru [24]. In 2016, the Lin group reported that some combinations of TCPP and tetrahedral $[In(COO)_4]$ units leads to a two-fold interpenetrated **pts** MOF (Figure 3C) [25]. Fe_3 clusters, a D_{3h} symmetry unit, can be connected through D_{4h} TCPP to afford a mesoporous **stp-a** network, PCN-600 [26], and the Fe_3 cluster can be replaced by Mg_3, Mn_3, Co_3, Ni_3, as well as mixed-metal clusters (Figure 3E) [27]. Moreover, Al can form 'infinite' Al-oxo chains with TCPP, in which two adjacent Al atoms are bridged by one OH and two COO groups, producing Al-PMOF with ABAB staggering of TCPP along the [010] direction (Figure 3D) [28]. Recently, an isostructural Ti-MOF DGIST-1 was reported by the Park group and μ_2-O was used in this MOF instead of μ_2-OH for charge balancing [29]. In addition, the topology of Zr-based porphyrin MOFs is versatile because the connectivity of Zr_6 clusters can be tuned to 6, 8, and 12, resulting in PCN-224 (**she**), PCN-222/MOF-545 (**csq**), and MOF-525 (**ftw-a**) (Figure 3F) [30-32]. There are also other isomers such as Zr-PCN-223 (**shp**)/NU-902 (**scu**), Zr-PCN-225 (**sqc**), and a rare earth-based analogue RE(rare earth)-**shp**-MOF that have been reported – a result of the various distortion angles of TCPP linkers during the framework formation process [33-36]. It is noted that the TCPP linker can be further extended, resulting in **ftw-a** networks PCN-228, PCN-229, and PCN-230 with enlarged pore apertures [37].

Looking back on the development of TCPP MOFs, their topologies highly depend on the metal-cluster geometry, which restricted the scope for potential MOFs. There are two strategies used to overcome limitations to design MOFs with novel topologies and properties. The first strategy is to introduce a secondary ligand to construct a mixed-ligand MOF. For instance, in 2018, Zhou, Sun, and coworkers synthesized a rare-earth (RE) MOF PCN-900 through incorporating auxiliary linker 4,4'-dicarboxydiphenyl sulfone (DCDPS) into RE-PCN-224 analogues, increasing the connectivity of RE_6 cluster from 6 to 12, and creating a network with **tam** topology [38]. Most recently, Zhou, Lan, Qin, and coworkers reported two mixed-ligand MOFs with face-sharing Archimedean solids stacking [56]. In this work, the combination of square (TCPP) and trigonal linkers resulted in two Archimedean solids rhombicuboctahedron and cuboctahedron, corresponding to **qyc** network PCN-137 and **urr** network PCN-138. The second strategy is to decrease the symmetry of TCPP (D_{4h}). For instance, the Ma group synthesized a tetratopic linker 5,15-

bis(3,5-dicarboxyphenyl)porphyrin (bdcpp) with D_{2h} symmetry, which could construct a **lvt** network MMPF-1 with Cu_2 paddlewheel clusters (Figure 3A) [40]. In 2019, Choe, Min, and coworkers reported a MOF UPF-1, in which C_4 linkers meso-tetra(3-carboxyphenyl)porphyrin (3-TCPP) and unprecedented 6-connected $[Zn_2(COO)_3]_2(\mu_2\text{-}O)$ clusters could form rhombicuboctahedron cages [39]. Most recently, Ma, Zhang, and coworkers synthesized corrole-MOFs with a rare **gfy** topology through a C_{2v} corrolic tricarboxylate ligand and D_{3d} 9-connected Zr_6/Hf_6 clusters [57]. This work indicated that porphyrin linkers with low symmetry have great potential for developing MOFs with novel topology.

Octatopic linkers such as tetrakis(3,5-dicarboxyphenyl)porphine (tdcpp) have attracted significant attention due to their high connectivity and symmetry. In 2012, Ma and coworkers reported two **pcu** networks formed with face-sharing packing of cubicuboctahedral nanocages, based on square tdcpp and triangular clusters $Zn_2(COO)_3$ or $Cd(COO)_3$ [41]. In the same year, Wu, Chen, and coworkers synthesized a **tbo** network ZJU-18 that was comprised of square tdcpp linkers and two 4-connected clusters $Mn_2(COO)_4$ and $[Mn_3(COO)_4(\mu_2\text{-}H_2O)_2]$ (Figure 3B) [42]. In 2014, Zhang and coworkers synthesized an anionic porphyrin MOF UNLPF-10 by connecting an extended octatopic ligand (tetrakis 3,5-bis[(4-carboxy)phenyl]phenylporphine (tbcppp) with 4-connected $[In(COO)_4]$ unit, leading to an unusual Williams *β*-tetrakaidecahedral cage [58].

While carboxylate-based linkers are the most common, several porphyrin MOFs with diverse bonding modes have been reported. For instance, in 2015, Zhou and coworkers reported a **scu-a** PCN-526 through 4-connected 5,10,15,20-tetrakis[4-(2H-tetrazol-5-yl)phenyl]porphyrin (TTPP) and 8-connected square $[Cd_4Cl]$ clusters [59]. In 2016, Zhou, Li, and coworkers synthesized a base-resistant **ftw-a** MOF PCN-601 based on tetratopic 5,10,15,20-tetra(1H-pyrazol-4-yl)-porphyrin (TPP) and 12-connected Ni_8 clusters [60]. PCN-601 was isostructural to MOF-525 and the TPP linker can be extended to 5,10,15,20-tetrakis(4-(1H-pyrazol-4-yl)-phenyl)porphyrin (TPPP), resulting in **ftw-a** PCN-602 [43]. Recently, Liu, Zhang, Bu, and coworkers reported two stable porphyrin MOFs ZrPP-1 and ZrPP-2 based on phenolic porphyrin linkers [61]. In this work, the 4-connected polyphenolic linker, 5,10,15,20-tetrakis(3,4,5-trihydroxyphenyl)porphyrin (THPP) or 5,10,15,20-tetrakis(3,4,5-trihydroxybiphenyl)porphyrin (THBPP), was connected to infinite Zr-oxo chains, generating a **nbo** topology. These works demonstrate that porphyrin linkers with multiple functional groups can generate rare clusters as well as novel topologies.

Synthesis and Structural Description of Porphyrin COFs

Covalent organic frameworks (COFs) are a class of emerging porous materials with high chemical and thermal stability, in which organic building units are bridged through covalent bonds [62]. The periodic framework and ordered arrangement of pore spaces in COFs allow for precise structural characterization using techniques such as electron

diffraction, single-crystal, or powder X-ray diffraction [63]. Similar to MOF chemistry, the topology and porosity of COFs can also be predesigned by controlling monomer geometry and connectivity. As a result of their planar structures and versatile properties, porphyrin linkers can serve as building blocks in the synthesis of functional COFs containing a *π*-conjugated system.

Most reported porphyrin COFs are based upon square porphyrin SBUs with C_4 symmetry. For instance, in 2011, Yaghi and coworkers reported a typical 2D porphyrin COF (COF-366) that was synthesized through condensation of tetra(*p*-amino-phenyl)porphyrin (TAPP) and terephthalaldehyde (TPA) [44]. The [4+2] combination of square and linear ligands resulted in a 2D **sql** network, in which TAPP linkers serve as the vertices while TPA is serves as the edge linker. Through reticular chemistry, the edge of COF-366 can be replaced elongated linkers such as 2,3,4,5-tetrahydroxy anthracene (THAn) and biphenyl-4,4'-dicarboxaldehyde (BPDA), leading to an extended **sql** network COF-66 and COF-367 [44, 45]. Besides, other porphyrin linkers like 5,10,15,20-tetrakis(4-benzaldehyde)porphyrin (TFPP) can be used as vertex linkers to construct a **sql** networks connected by p-phenylenediamine [64]. It should be noted that the functionality of porphyrin COFs can be tuned by incorporating versatile linear linkers into the framework, resulting in unique structures such as enforced porphyrin J-aggregates [51] and hydrogen-bonding locked layers [48].

Although the COFs mentioned above are all connected through imine bonds, other dynamic covalent bonds can be utilized to construct porphyrin COFs. For instance, in 2012, Jiang and coworkers reported a **sql** COF that was connected through a boron-oxygen bond via a [4+2] condensation between 5, 10, 15, 20-tetrakis[4-(dihydroxyboryl)phenyl]porphine (TBP) and 1,2,4,5-tetrahydroxybenzene (THB) [46]. In 2016, the Xu group reported a **sql** azodioxy-linked COF via polymerization of a protected tetrakis(arylhydroxylamine)porphyrin [65]. In 2017, a polyimide COF (PI-COF) was prepared by the Xian group *via* [4+2] condensation of TAPP and perylenetracarboxylic dianhydride (PTCA) [66]. Recently, the Wang group reported a sp^2-carbon-conjugated COF that was synthesized through Knoevenagel condensation between TFPP and 1,4-phenylenediacetonitrile (PDAN), in which the C=C linkages endowed the COF with stability under various conditions [54].

A [4+4] strategy can be applied to fabricate **sql** COFs. For instance, COF-420, first reported by Joshi and coworkers, was synthesized through a Schiff base type condensation of TAPP and TFPP [52, 53]. The connection between the two square planar precursors yielded a 2D **sql** network with heterojunctions. In 2017, Bhunia and coworkers prepared a **sql** COF through a Schiff base-type condensation between TAPP and a pyrene ligand TFFPy (1,3,6,8-tetrakis(4-formylphenyl) pyrene) [50]. Interestingly, the combination of square and rectangle building blocks distorted the 2D layers and yielded a quasi-two-dimensional COF. In 2019, the Lan group synthesized a TTCOF based on TAPP and 2,3,6,7-tetra(4-formylphenyl)-tetrathiafulvalene (TTF), which was a rectangular building block as well [55].

As most reported porphyrin COFs feature a **sql** topology, it is imperative to construct porphyrin COFs with diverse topologies, which can be achieved through tuning the building block geometry. For instance, in 2014, the Bein group reported a **hcb** layered TP-Por COF through [2+3] condensation of a linear linker bis(boronophenyl)porphyrin (BBP) and a trigonal linker 2,3,6,7,10,11-hexahydroxytriphenylene (HHTP) [47]. The honeycomb-like 2D COF contains hexagonal pores with a diameter of 4.6 nm, in which the porphyrin subunits are the edge and the triphenylene subunits are the vertex. In 2017, through [4+4] imine condensation of a square linker TFPP and a tetrahedral linker tetra(*p*-aminophenyl)methane (TAPM), Wang and coworkers synthesized the first 3D porphyrin COF with a **pts** topology [49]. The 3D-Por-COF features micro-porosity and a 2-fold interpenetrated structure, paving a new way for design of novel 3D porphyrin COFs.

Applications in Catalysis

Lewis Acid Catalysis

Porphyrins with unsaturated metal centers within framework compounds can function as efficient Lewis acid catalysts by offering available coordination sites and facilitating the catalytic transformation within open pore spaces of framework compounds (Table 2). One model reaction is the ring-opening of styrene epoxide with trimethylsilylazide ($TMSN_3$). Takaishi, Farha, Hupp, and coworkers reported a Zn-based porphyrin MOF (ZnAl-RPM) that could catalyze this ring-opening reaction efficiently due to the strong Lewis acidity of Al(III) sites in the porphyrin linkers [67]. Later, Stoddart, Cramer, Hupp, and Farha designed a **tandem catalytic** system that couples a Fe-porphyrin catalyzed epoxidation of styrene with a subsequent Hf_6 cluster catalyzed epoxide opening by using a recyclable heterogeneous PCN-222/MOF-545(Hf) catalyst (Figure 4A) [68]. Another typical Lewis acid-catalyzed reaction is the widely studied CO_2 cycloaddition reaction. Zhou and coworkers studied the performance of PCN-224(Co) for the generation of cyclic carbonates through CO_2 cycloaddition at 100 ˚C under 2 MPa. It was found that PCN-224(Co) demonstrated high activity and recyclability due to the presence of Lewis acidic sites in both the porphyrin centers and Zr_6 clusters [30]. Furthermore, multiple Lewis acidic metal sites can be sequentially placed on the linear linker and the tetratopic porphyrinic linker of a RE-based porphyrinic MOF (PCN-900) leading to high catalytic cycloaddition activity [38]. Very recently, Zhang, Ma, and coworkers reported a corrole-based Zr-MOF with a (3, 9)-connected **gfy** net [57]. The corrole-based MOF demonstrated highly efficient Lewis acid catalytic activity over a [4+2] hetero-Diels–Alder (HDA) reaction, bypassing the performance of the homogeneous counterpart and the porphyrinic counterpart PCN-224(Fe).

Oxidation Catalysis

Metalloporphyrins in framework compounds can efficiently catalyze the oxidization of various organic molecules [72, 73]. Jiang and coworkers introduced Pt nanocrystals into porphyrinic PCN-224(M) to selective oxidize aromatic alcohols to aldehydes at ambient

temperature. The oxidization reaction can achieve excellent selectivity without involving harsh chemicals or high pressure, due to a synergistic effect within Pt/PCN-224(M) composites such as photothermal effects of both Pt and PCN-224, surface electronic state of Pt nanocrystals, and diamagnetism of PCN-224(M) porphyrin metal center [74]. The pore environment of porphyrin framework compounds can also be decorated with functional groups with electron-donating and electron-withdrawing properties such as ethyl, bromo, chloro, and fluoro groups, that can enhance the molecular-level understanding on the importance of chemical environment around a catalytic center during heterogeneous catalysis [75]. Zhou and coworkers prepared a series of isostructural PCN-224 analogues with different substitutes on porphyrin rings that shown an extremely high activity, selectivity, and recyclability for 3-methylpentane oxidation (Figure 4B) [69].

Photocatalysis

As a highly conjugated aromatic electron system, porphyrins and metalloporphyrins exhibit distinct chromophoric properties and superior photocatalytic activities in both homogeneous and heterogeneous reactions [58, 78-80]. One of remarkable examples is reported by Jiang and coworkers (Figure 4C) [70]. Under visible-light irradiation, porphyrinic PCN-222 shown enhanced photocatalytic conversion activity of CO_2 into formate anions (30 μmol in 10 h) because there exists an extremely long-lived electron trap state in PCN-222 that prevents the unwanted electron-hole recombination observed in most porphyrin ligands. This work highlights the potential of assembling porphyrinic units into framework materials as heterogeneous catalysts. Experiments have shown that the core metals in the porphyrin ring play a vital role in photocatalytic CO_2 reduction. Ye and coworkers found that MOF-525-Co demonstrated an enhanced reactivity compared to its undoped counterpart, as a result of directional migration of photogenerated excitons from the porphyrin to the metal core [76]. A Zr-polyphenolate framework containing Co-porphyrin has also been tested and has demonstrated high activity and selectivity for photoreduction of CO_2 under visible-light irradiation [61].

Lan and coworkers reported a series of 2D COFs constructed from electron-deficient metalloporphyrin and electron-rich tetrathiafulvalene (TTF), which were further used for artificial photosynthesis by reducing CO_2 with H_2O [55]. The covalent coupling between porphyrin building blocks with potential CO2 reduction ability, and TTF, allows for rapid electron transfer within the framework of COFs and leads to the separation and transfer of visible-light driven electrons. Further reduction and oxidation reactions can proceed with a high yields and high selectivity of CO, with O_2 as the oxidized product. There have also been cases of porphyrin-based COFs, such as imine linked or sp^2 carbon-conjugated porphyrin COFs, that demonstrate both high recyclability and photocatalytic performance [54].

Electrocatalysis

Redox-active porphyrins can be incorporated into framework compounds for enhanced performance of electrochemical carbon dioxide reduction reactions (CO2RR) [81-83]. Yang, Yaghi, and coworkers prepared nanosized $Al_2(OH)_2$TCPP-Co thin films *via* atomic-layer deposition (ALD) and used them as catalysts for electrochemical CO2 reduction (Figure 4E) [71]. As a result, a high CO selectivity of over 76% over 7 h was achieved by the MOF electrode, while the reduction of Co(II) to Co(I) in the porphyrin linker center was observed during CO_2 reduction. Subsequent aqueous electrochemical reduction of CO_2 to CO utilizing porphyrin framework compounds was reported by Chang, Yaghi, and coworkers. By optimizing the metal composition and ratio in porphyrin rings, COFs containing cobalt porphyrin catalysts connected by imine bonds exhibited superior Faradaic efficiency (90%), turnover numbers and stability with minimal degradation over 24 h (Figure 4D) [45]. They also demonstrated that by modifying the environment of catalytic Co-porphyrin sites, the electronic connectivity between the Co-porphyrin active sites and surrounding functional groups can be optimized, thus leading to the high selectivity and efficiency of the resultant system [77]. In addition, Zhang and coworkers utilized a one-pot synthesis to fabricate porphyrin framework compounds, and the Co framework has shown superior bifunctional electrocatalytic performances for oxygen reduction reaction (ORR) and oxygen evolution reaction (OER) [84].

Concluding Remarks

In summary, we discuss the structures and recent catalytic applications of porphyrin framework compounds that have been studied over the last decade. Extensive efforts have been made to design porphyrinic building blocks with various sizes, geometries, connectivity, substituents, and functional groups, which are then used as linkers in MOFs and monomers in COFs. The efficient synthetic strategies, guided by reticular chemistry for the construction of porphyrin framework compounds were introduced, leading to the discovery of an extensive and diverse porphyrin family for cutting-edge catalytic applications. Benefiting from the redox properties and functional versatility of porphyrins, porphyrin framework compounds exhibited significant advantages as Lewis acid catalysts, oxidation catalysts, photocatalysts, and electrocatalysts. Of special note are porphyrin framework compounds with tailored pore environments, which have recently demonstrated potential for photocatalytic and electrochemical reduction of CO_2, converting these into high value chemicals. Here, we highlight some potential directions that can be explored in the advancement of porphyrin framework compounds for catalysis.

Currently, the design and construction of porphyrin building blocks in MOFs and COFs relies primarily on high symmetry guided design, which limits the diversity of the porphyrin framework family and affects their potential catalytic applications. Introducing desymmetrization strategies into the design should introduce novel functions of these

framework materials [85]. By altering the sizes, geometries, and substituents asymmetrically, porphyrin building blocks with unusual connectivity numbers (such as three, five, seven, or higher), unusual geometries (trapezoid, rhombus, pivot–hinge, or others) and unsymmetrical substituents can be utilized to construct framework materials (see Outstanding Questions). Higher complexity of porphyrin framework compounds can be enhanced by utilizing known organometallic reactions into the preparation process of porphyrin ligands such as diporphyrin, triporphyrin, and other porphyrin oligomers [86]. In addition, to further enhance the diversity of porphyrin framework compounds, using mixed rigid porphyrin building blocks and other relatively flexible linkers can be viewed as an effective synthetic method. The auxiliary linkers with varying sizes, connectivity and flexibility should play a vital role not only in framework assembly but also in functional cooperativity.

Another potential avenue is investigation of the amorphization of porphyrin framework compounds. Due to the harsh catalytic conditions and relatively labile nature of certain frameworks, transformation of crystalline porphyrin framework compounds into amorphous porphyrin materials were observed in some of these materials. The mechanism of this amorphization and the influence of amorphization on the overall catalytic activity and recyclability during the catalysis should be the primary focus.There are also some reported amorphous coordination polymers and organic polymers that are synthesized via a one-pot polymerization, and their performance should be studied in comparison with that of crystalline framework materials.

The large planar structure of porphyrin building blocks ensures the strong π interactions with guest molecules. Coupling the porphyrin framework compounds with other guests can lead to the cooperative properties in the confined pore environment. For example, Zhang, Lu, and coworkers reported the encapsulation of perovskite quantum dots $CH_3NH_3PbI_3$ in porphyrinic PCN-221(Fe), which exhibits enhanced photocatalytic CO_2 reduction activity [87]. Lan and coworkers studied the introduction of polyoxometalate into porphyrinic framework materials for highly selective photoreduction and electroreduction of CO_2 [88, 89]. We expect that more novel porphyrin framework compounds and their composites will be discovered and synthesized, which shall bring new opportunities for sophisticated catalytic conversion with unusual synergism.

Acknowledgements

We would like to thank the support of the Center for Gas Separations, an Energy Frontier Research Center funded by the U. S. Department of Energy, Office of Science, and Office of Basic Energy Sciences under Award Number DE-SC0001015, and the Robert A. Welch Foundation through a Welch Endowed Chair to H.-C. Z. (A-0030).

Disclaimer Statement
The authors declare no competing interest.

Glossary

Building block: Organic linkers or metal clusters serving as joints in framework compounds.

Covalent organic framework (COF): Porous, crystalline two-dimensional or three-dimensional polymers connected by covalent bonds.

Interpenetration: Intergrowth of a secondary framework within the voids of a parent framework.

Isostructure: Two framework compounds with the same topology, derived from similar connectivity and geometry of building units.

Metal-organic framework (MOF): A porous and crystalline coordination polymer comprised of organic linkers and metal nodes or clusters. Alternative names include porous coordination network (PCN) and porous coordination polymer (PCP).

Tandem catalysis: A one-pot catalytic approach involving two or more catalysts, in which a comonomer is produced by the first catalyst and enters the following catalytic process of other catalysts to produce the final products.

Topology: A simplified representation to describe connectivity and continuity of a molecule or a network. The topologies of networks can be represented in three-letter codes.

References

1. Jasat, A. and Dolphin, D. (1997) Expanded porphyrins and their heterologs. Chem. Rev. 97 (6), 2267-2340.
2. Mack, J. (2016) Expanded, contracted, and isomeric porphyrins: theoretical aspects. Chem. Rev. 117 (4), 3444-3478.
3. Tanaka, T. and Osuka, A. (2016) Chemistry of meso-aryl-substituted expanded porphyrins: aromaticity and molecular twist. Chem. Rev. 117 (4), 2584-2640.
4. Singh, S. et al. (2015) Glycosylated Porphyrins, Phthalocyanines, and Other Porphyrinoids for Diagnostics and Therapeutics. Chem. Rev. 115 (18), 10261-10306.
5. Urbani, M. et al. (2014) Meso-Substituted Porphyrins for Dye-Sensitized Solar Cells. Chem. Rev. 114 (24), 12330-12396.
6. Dolgopolova, E.A. et al. (2018) Photochemistry and photophysics of MOFs: steps towards MOF-based sensing enhancements. Chem. Soc. Rev. 47 (13), 4710-4728.
7. Gao, W.-Y. et al. (2014) Metal–metalloporphyrin frameworks: a resurging class of functional materials. Chem. Soc. Rev. 43 (16), 5841-5866.
8. Simon-Yarza, T. et al. (2018) Nanoparticles of Metal-Organic Frameworks: On the Road to In Vivo Efficacy in Biomedicine. Adv. Mater. 30 (37).

9. Cohen, S.M. (2012) Postsynthetic Methods for the Functionalization of Metal-Organic Frameworks. Chem. Rev. 112 (2), 970-1000.
10. Kirchon, A. et al. (2018) From fundamentals to applications: a toolbox for robust and multifunctional MOF materials. Chem. Soc. Rev. 47 (23), 8611-8638.
11. Lee, J. et al. (2009) Metal-organic framework materials as catalysts. Chem. Soc. Rev. 38 (5), 1450-1459.
12. Yuan, S. et al. (2018) Stable Metal–Organic Frameworks: Design, Synthesis, and Applications. Adv. Mater.
13. Feng, L. et al. (2019) Porphyrinic Metal–Organic Frameworks Installed with Brønsted Acid Sites for Efficient Tandem Semisynthesis of Artemisinin. ACS Catal. 9 (6), 5111-5118.
14. Furukawa, H. et al. (2010) Ultrahigh porosity in metal-organic frameworks. Science 329 (5990), 424-8.
15. Liu, Y.Z. et al. (2016) Weaving of organic threads into a crystalline covalent organic framework. Science 351 (6271), 365-369.
16. Helal, A. et al. (2017) Multivariate metal-organic frameworks. Natl. Sci. Rev. 4 (3), 296-298.
17. Li, H. et al. (1999) Design and synthesis of an exceptionally stable and highly porous metal-organic framework. Nature 402 (6759), 276-279.
18. Zhai, Q.G. et al. (2017) Pore Space Partition in Metal-Organic Frameworks. Acc. Chem. Res. 50 (2), 407-417.
19. Feng, L. et al. (2018) Uncovering Two Principles of Multivariate Hierarchical Metal-Organic Framework Synthesis via Retrosynthetic Design. ACS Cent. Sci. 4 (12), 1719-1726.
20. Gao, W.Y. et al. (2016) Interpenetrating Metal-Metalloporphyrin Framework for Selective CO2 Uptake and Chemical Transformation of CO2. Inorg. Chem. 55 (15), 7291-7294.
21. Lu, K.D. et al. (2014) Nanoscale Metal-Organic Framework for Highly Effective Photodynamic Therapy of Resistant Head and Neck Cancer. J. Am. Chem. Soc. 136 (48), 16712-16715.
22. Micheroni, D. et al. (2018) Efficient Electrocatalytic Proton Reduction with Carbon Nanotube-Supported Metal-Organic Frameworks. J. Am. Chem. Soc. 140 (46), 15591-15595.
23. Makiura, R. et al. (2010) Surface nano-architecture of a metal-organic framework. Nat. Mater. 9 (7), 565-571.
24. Lan, G.X. et al. (2018) Electron Injection from Photoexcited Metal-Organic Framework Ligands to Ru-2 Secondary Building Units for Visible-Light-Driven Hydrogen Evolution. J. Am. Chem. Soc. 140 (16), 5326-5329.
25. Lin, Z.K. et al. (2016) Highly Efficient Cooperative Catalysis by Co-III(Porphyrin) Pairs in Interpenetrating Metal-Organic Frameworks. Angew. Chem. Int. Ed. 55 (44), 13739-13743.
26. Wang, K.C. et al. (2014) A Series of Highly Stable Mesoporous Metalloporphyrin Fe-MOFs. J. Am. Chem. Soc. 136 (40), 13983-13986.
27. Liu, Q. et al. (2016) Deciphering the Spatial Arrangement of Metals and Correlation to Reactivity in Multivariate Metal-Organic Frameworks. J. Am. Chem. Soc. 138 (42), 13822-13825.

28. Fateeva, A. et al. (2012) A Water-Stable Porphyrin-Based Metal-Organic Framework Active for Visible-Light Photocatalysis. Angew. Chem. Int. Ed. 51 (30), 7440-7444.
29. Keum, Y. et al. (2018) Titanium-Carboxylate Metal-Organic Framework Based on an Unprecedented Ti-Oxo Chain Cluster. Angew. Chem. Int. Ed. 57 (45), 14852-14856.
30. Feng, D.W. et al. (2013) Construction of Ultrastable Porphyrin Zr Metal-Organic Frameworks through Linker Elimination. J. Am. Chem. Soc. 135 (45), 17105-17110.
31. Feng, D.W. et al. (2012) Zirconium-Metalloporphyrin PCN-222: Mesoporous Metal-Organic Frameworks with Ultrahigh Stability as Biomimetic Catalysts. Angew. Chem. Int. Ed. 51 (41), 10307-10310.
32. Morris, W. et al. (2012) Synthesis, Structure, and Metalation of Two New Highly Porous Zirconium Metal-Organic Frameworks. Inorg. Chem. 51 (12), 6443-6445.
33. Chen, Z.J. et al. (2017) Applying the Power of Reticular Chemistry to Finding the Missing alb-MOF Platform Based on the (6,12)-Coordinated Edge -Transitive Net. J. Am. Chem. Soc. 139 (8), 3265-3274.
34. Jiang, H.L. et al. (2013) An Exceptionally Stable, Porphyrinic Zr Metal-Organic Framework Exhibiting pH-Dependent Fluorescence. J. Am. Chem. Soc.135 (37), 13934-13938.
35. Deria, P. et al. (2016) Framework-Topology-Dependent Catalytic Activity of Zirconium-Based (Porphinato)zinc(II) MOFs. J. Am. Chem. Soc.138 (43), 14449-14457.
36. Feng, D.W. et al. (2014) A Highly Stable Porphyrinic Zirconium Metal-Organic Framework with shp-a Topology. J. Am. Chem. Soc.136 (51), 17714-17717.
37. Liu, T.F. et al. (2015) Topology-Guided Design and Syntheses of Highly Stable Mesoporous Porphyrinic Zirconium Metal-Organic Frameworks with High Surface Area. J. Am. Chem. Soc.137 (1), 413-419.
38. Zhang, L.L. et al. (2018) Pore-Environment Engineering with Multiple Metal Sites in Rare-Earth Porphyrinic Metal-Organic Frameworks. Angew. Chem. Int. Ed. 57 (18), 5095-5099.
39. Jin, E. et al. (2019) Metal-organic framework based on hinged cube tessellation as transformable mechanical metamaterial. Sci. Adv. 5 (5).
40. Wang, X.S. et al. (2011) Three-dimensional porous metal-metalloporphyrin framework consisting of nanoscopic polyhedral cages. J. Am. Chem. Soc.133 (41), 16322-5.
41. Wang, X.S. et al. (2012) Vertex-directed self-assembly of a high symmetry supermolecular building block using a custom-designed porphyrin. Chem Sci 3 (9), 2823-2827.
42. Yang, X.L. et al. (2012) Porous Metalloporphyrinic Frameworks Constructed from Metal 5,10,15,20-Tetrakis(3,5-biscarboxylphenyl)porphyrin for Highly Efficient and Selective Catalytic Oxidation of Alkylbenzenes. J Am Chem Soc 134 (25), 10638-10645.
43. Lv, X.L. et al. (2017) A Base-Resistant Metalloporphyrin Metal-Organic Framework for C-H Bond Halogenation. J. Am. Chem. Soc.139 (1), 211-217.
44. Wan, S. et al. (2011) Covalent Organic Frameworks with High Charge Carrier Mobility. Chem. Mater. 23 (18), 4094-4097.
45. Lin, S. et al. (2015) Covalent organic frameworks comprising cobalt porphyrins for catalytic CO2 reduction in water. Science 349 (6253), 1208-1213.

46. Feng, X. et al. (2012) High-Rate Charge-Carrier Transport in Porphyrin Covalent Organic Frameworks: Switching from Hole to Electron to Ambipolar Conduction. Angew. Chem. Int. Ed. 51 (11), 2618-2622.
47. Calik, M. et al. (2014) Extraction of Photogenerated Electrons and Holes from a Covalent Organic Framework Integrated Heterojunction. J. Am. Chem. Soc. 136 (51), 17802-17807.
48. Chen, X. et al. (2015) Locking Covalent Organic Frameworks with Hydrogen Bonds: General and Remarkable Effects on Crystalline Structure, Physical Properties, and Photochemical Activity. J. Am. Chem. Soc. 137 (9), 3241-3247.
49. Lin, G.Q. et al. (2017) 3D Porphyrin-Based Covalent Organic Frameworks. J. Am. Chem. Soc. 139 (25), 8705-8709.
50. Bhunia, S. et al. (2017) Electrochemical Stimuli-Driven Facile Metal-Free Hydrogen Evolution from Pyrene-Porphyrin-Based Crystalline Covalent Organic Framework. ACS Appl. Mater. Inter. 9 (28), 23843-23851.
51. Keller, N. et al. (2018) Enforcing Extended Porphyrin J-Aggregate Stacking in Covalent Organic Frameworks. J. Am. Chem. Soc. 140 (48), 16544-16552.
52. Joshi, T. et al. (2019) Local Electronic Structure of Molecular Heterojunctions in a Single-Layer 2D Covalent Organic Framework. Adv. Mater. 31 (3).
53. Biswal, B.P. et al. (2019) Nonlinear Optical Switching in Regioregular Porphyrin Covalent Organic Frameworks. Angew. Chem. Int. Ed. 58 (21), 6896-6900.
54. Chen, R.F. et al. (2019) Designed Synthesis of a 2D Porphyrin-Based sp(2) Carbon-Conjugated Covalent Organic Framework for Heterogeneous Photocatalysis. Angew. Chem. Int. Ed. 58 (19), 6430-6434.
55. Lu, M. et al. (2019) Rational Design of Crystalline Covalent Organic Frameworks for Efficient CO2 Photoreduction with H2O. Angew. Chem. Int. Ed.
56. Qiu, Y.C. et al. (2019) Face-Sharing Archimedean Solids Stacking for the Construction of Mixed-Ligand Metal-Organic Frameworks. J. Am. Chem. Soc. 141 (35), 13841-13848.
57. Zhao, Y. et al. (2019) Robust Corrole-Based Metal-Organic Frameworks with Rare 9-Connected Zr/Hf-Oxo Clusters. J. Am. Chem. Soc. 141 (36), 14443-14450.
58. Johnson, J.A. et al. (2014) Facile Control of the Charge Density and Photocatalytic Activity of an Anionic Indium Porphyrin Framework via in Situ Metalation. J. Am. Chem. Soc. 136 (45), 15881-15884.
59. Liu, D.H. et al. (2015) A Reversible Crystallinity-Preserving Phase Transition in Metal Organic Frameworks: Discovery, Mechanistic Studies, and Potential Applications. J. Am. Chem. Soc. 137 (24), 7740-7746.
60. Wang, K.C. et al. (2016) Pyrazolate-Based Porphyrinic Metal-Organic Framework with Extraordinary Base-Resistance. J. Am. Chem. Soc. 138 (3), 914-919.
61. Chen, E.X. et al. (2018) Acid and Base Resistant Zirconium Polyphenolate-Metalloporphyrin Scaffolds for Efficient CO2 Photoreduction. Adv. Mater. 30 (2).
62. Cote, A.P. et al. (2005) Porous, crystalline, covalent organic frameworks. Science 310 (5751), 1166-1170.
63. Ma, T.Q. et al. (2018) Single-crystal x-ray diffraction structures of covalent organic frameworks. Science 361 (6397), 48-52.
64. Liao, H.P. et al. (2016) A 2D porous porphyrin-based covalent organic framework for sulfur storage in lithium sulfur batteries. J. Mater. Chem. A 4 (19), 7416-7421.

65. Nath, B. et al. (2016) A new azodioxy-linked porphyrin-based semiconductive covalent organic framework with I-2 doping-enhanced photoconductivity. Crystengcomm 18 (23), 4259-4263.
66. Zhang, C.L. et al. (2017) Highly Fluorescent Polyimide Covalent Organic Nanosheets as Sensing Probes for the Detection of 2,4,6-Trinitrophenol. ACS Appl. Mater. Inter. 9 (15), 13415-13421.
67. Takaishi, S. et al. (2013) Solvent-assisted linker exchange (SALE) and post-assembly metallation in porphyrinic metal-organic framework materials. Chem. Sci. 4 (4), 1509-1513.
68. Beyzavi, M.H. et al. (2015) A Hafnium-Based Metal-Organic Framework as a Nature-Inspired Tandem Reaction Catalyst. J. Am. Chem. Soc. 137 (42), 13624-13631.
69. Huang, N. et al. (2017) Systematic Engineering of Single Substitution in Zirconium Metal-Organic Frameworks toward High-Performance Catalysis. J. Am. Chem. Soc.139 (51), 18590-18597.
70. Xu, H.Q. et al. (2015) Visible-Light Photoreduction of CO2 in a Metal-Organic Framework: Boosting Electron-Hole Separation via Electron Trap States. J. Am. Chem. Soc. 137 (42), 13440-13443.
71. Kornienko, N. et al. (2015) Metal-Organic Frameworks for Electrocatalytic Reduction of Carbon Dioxide. J. Am. Chem. Soc. 137 (44), 14129-14135.
72. Huang, N. et al. (2018) Flexible and Hierarchical Metal-Organic Framework Composites for High-Performance Catalysis. Angew. Chem. Int. Ed. 57 (29), 8916-8920.
73. Feng, L. et al. (2019) Temperature-Controlled Evolution of Nanoporous MOF Crystallites into Hierarchically Porous Superstructures. Chem 5 (5), 1265-1274.
74. Chen, Y.Z. et al. (2017) Singlet Oxygen-Engaged Selective Photo-Oxidation over Pt Nanocrystals/Porphyrinic MOF: The Roles of Photothermal Effect and Pt Electronic State. J. Am. Chem. Soc. 139 (5), 2035-2044.
75. Xiao, D.N.J. et al. (2016) Pore Environment Effects on Catalytic Cyclohexane Oxidation in Expanded Fe-2(dobdc) Analogues. J Am Chem Soc 138 (43), 14371-14379.
76. Zhang, H.B. et al. (2016) Efficient Visible-Light-Driven Carbon Dioxide Reduction by a Single-Atom Implanted Metal-Organic Framework. Angew. Chem. Int. Ed. 55 (46), 14308-14312.
77. Diercks, C.S. et al. (2018) Reticular Electronic Tuning of Porphyrin Active Sites in Covalent Organic Frameworks for Electrocatalytic Carbon Dioxide Reduction. J. Am. Chem. Soc. 140 (3), 1116-1122.
78. Knor, G. (1998) Photocatalytic reactions of porphyrin-based multielectron transfer sensitizers. Coordin. Chem. Rev. 171, 61-70.
79. Hong, Y.H. et al. (2019) Photocatalytic Oxygenation Reactions with a Cobalt Porphyrin Complex Using Water as an Oxygen Source and Dioxygen as an Oxidant. J. Am. Chem. Soc. 141 (23), 9155-9159.
80. Rosenthal, J. et al. (2006) Photocatalytic oxidation of hydrocarbons by a bis-iron(III)-mu-oxo Pacman porphyrin using O-2 and visible light. J. Am. Chem. Soc.128 (20), 6546-6547.
81. Kaminsky, C.J. et al. (2019) Graphite-Conjugation Enhances Porphyrin Electrocatalysis. ACS Catal. 9 (4), 3667-3671.
82. Su, B. et al. (2010) Molecular Electrocatalysis for Oxygen Reduction by Cobalt Porphyrins Adsorbed at Liquid/Liquid Interfaces. J. Am. Chem. Soc. 132 (8), 2655-2662.

83. Yu, H.Z. et al. (1999) Femtosecond dynamics and electrocatalysis of the reduction of O-2: Tetraruthenated cobalt porphyrins. J. Am. Chem. Soc. 121 (2), 484-485.
84. Li, B.Q. et al. (2019) One-Pot Synthesis of Framework Porphyrin Materials and Their Applications in Bifunctional Oxygen Electrocatalysis. Adv. Funct. Mater. 29 (29).
85. Feng, L. et al. (2019) Molecular Pivot-Hinge Installation to Evolve Topology in Rare-Earth Metal–Organic Frameworks. Angew. Chem. Int. Ed.
86. Hiroto, S. et al. (2017) Synthesis and Functionalization of Porphyrins through Organometallic Methodologies. Chem. Rev. 117 (4), 2910-3043.
87. Wu, L.Y. et al. (2019) Encapsulating Perovskite Quantum Dots in Iron-Based Metal-Organic Frameworks (MOFs) for Efficient Photocatalytic CO2 Reduction. Angew. Chem. Int. Ed. 58 (28), 9491-9495.
88. Huang, Q. et al. (2019) Multielectron transportation of polyoxometalate-grafted metalloporphyrin coordination frameworks for selective CO2-to-CH4 photoconversion. Nat. Sci. Rev.
89. Wang, Y.-R. et al. (2018) Oriented electron transmission in polyoxometalate-metalloporphyrin organic framework for highly selective electroreduction of CO2. Nat. Commun. 9 (1), 4466.

Table 1. Summary of representative porphyrin framework materials and their applications.[a]

MOF	Topology	Organic linker	Metal cluster/chain	Applications	Ref.
NAFS-1	sql	4-c TCPP	4-c $[Cu_2(COO)_4]$	-	[23]
Al-PMOF	-	4-c TCPP	$[Al(\mu_2\text{-}OH)(COO)_2]$ chain	Photocatalytic hydrogen evolution	[28]
PCN-222	csq	4-c TCPP	8-c $[Zr_6(\mu_3\text{-}O)_4(\mu_3\text{-}OH)_4(OH)_4(H_2O)4(COO)_8]$	Biomimetic catalysis	[31]
PCN-224	she	4-c TCPP	6-c $[Zr_6(\mu_3\text{-}O)_4(\mu_3\text{-}OH)_4(OH)_6(H_2O)_6(COO)_6]$	CO_2/epoxide coupling reaction	[30]
PCN-228	ftw	4-c TCP-1	12-c $[Zr_6(\mu_3\text{-}O)_4(\mu_3\text{-}OH)_4(COO)_{12}]$	-	[37]
In-Co(TBP)-MOF	pts	4-c TCPP	4-c $[In(COO)_4]$	Cooperative catalysis	[25]
PCN-600	stp	4-c TCPP	6-c $[Fe_3(\mu_3\text{-}O)(COO)_6]$	Enzyme-mimetic catalysis	[26, 27]
PCN-900	tam	4-c TCPP/ 2-c DCDPS	12-c $[RE_6(OH)_8(COO)_{12}]$	CO_2 cycloaddition	[38]
UPF-1	-	4-c 3-TCPP/ 2-c BPY	6-c $[Zn_2(COO)_3]_2(\mu_2\text{-}O)$	Negative Poisson's ratio material	[39]
MMPF-1	lvt	4-c bdcpp	4-c $[Cu_2(COO)_4]$	Selective gas adsorption	[40]
MMPF-4	pcu	8-c tdcpp	3-c $[Zn_2(COO)_3]$	CO_2 adsorption	[41]
ZJU-18	tbo	8-c tdcpp	4-c $Mn_2(COO)_4$ /4-c $[Mn_3(COO)_4(\mu_2\text{-}H_2O)_2]$	Catalytic oxidation of alkylbenzene	[42]
PCN-602	ftw	4-c TPPP	12-c $[Ni_8(OH)_4(H_2O)_2Pz_{12}]$	C-H bond halogenation	[43]
Hf_{12}-CoDBP	hcp	2-c CoDBP	18-c $[Zr_{12}O_8(\mu_3\text{-}OH)_4(\mu_2\text{-}OH)_6\ (COO)_{18}]$	Electrocatalytic proton reduction	[22]
COF	**Topology**	**Component I**	**Component II**	**Applications**	**Ref.**
COF-366	sql	TAPP	TPA	Electrical conductivity	[44]
COF-367	sql	TAPP	BPDA	CO_2 reduction	[45]
H_2P-COF	sql	TBP	THB	Photoconductivity	[46]
TP-Por COF	hcb	BBP	HHTP	Photovoltaic devices	[47]
H_2P-DHPh-COF	sql	TAPP	DHTA	Photocatalysis	[48]
3D-Por-COF	pts	TFPP	TAPM	Photocatalysis	[49]
SB-PORPy-COF	sql	TAPP	TFFPy	Hydrogen evolution	[50]
TT-Por COF	sql	TAPP	TT	Photoluminescence	[51]
COF-420	sql	TAPP	TFPP	Nonlinear optical switching	[52, 53]
Por-sp^2c-COF	sql	TFPP	PDAN	Photocatalysis	[54]
TTCOF-2H	sql	TAPP	TTF	CO_2 reduction	[55]

[a] Ligands are abbreviated as: TCPP = tetrakis(4-carboxyphenyl)porphyrin; DCDPS = 4,4'-dicarboxydiphenyl sulfone; 3-TCPP = meso-tetra(3-carboxyphenyl)porphyrin; BPY = 4,4'-bipyridine; bdcpp = 5,15-bis(3,5-dicarboxyphenyl)porphyrin; tdcpp = tetrakis(3,5-dicarboxyphenyl)porphine; TPPP = 5,10,15,20-tetrakis(4-(pyrazolate-4-yl)-phenyl)porphyrin; Pz = pyrazolate; CoDBP = Co-metalated 5,15-di(p-benzoato)porphyrin; TAPP = tetra(*p*-amino-phenyl)porphyrin; TPA = terephthalaldehyde; H_2P = 5, 10, 15, 20-tetrakis[4-(dihydroxyboryl)phenyl]porphine; BPDA = biphenyl-4,4'-dicarboxaldehyde; THB = 1,2,4,5-tetrahydroxybenzene; BBP = bis(boronophenyl)porphyrin; HHTP = 2,3,6,7,10,11-hexahydroxytriphenylene; DHTA = dihydroxyterephthalaldehyde; TFPP = 5,10,15,20-tetrakis(4-benzaldehyde)porphyrin; TAPM = tetra(p-aminophenyl)methane; TFFPy = 1,3,6,8-tetrakis(4-formylphenyl) pyrene; TT = thieno[3,2-*b*]thiophene-2,5-dicarboxaldehyde; PDAN = 1,4-phenylenediacetonitrile; TTF = 2,3,6,7-tetra(4-formylphenyl)-tetrathiafulvalene.

Table 2. Summary of representative catalytic porphyrin frameworks and their performance.

MOF/COF	Application	Reaction Type	Conversion	Selectivity/Efficiency	Ref.
ZnAl-RPM	Lewis acid catalysis	Ring-opening reaction	60%	73%	[67]
PCN-222/MOF-545(Hf)	Lewis acid catalysis & Oxidation catalysis	Tandem reaction	>99%	>99%	[68]
PCN-224(Co)	Lewis acid catalysis	CO_2 cycloaddition	42%	TOF = 115 h^{-1}	[30]
PCN-900	Lewis acid catalysis	CO_2 cycloaddition	98%	-	[38]
Corrole-MOF-1(Fe)	Lewis acid catalysis	Hetero-Diels–Alder reaction	96%	-	[57]
In-Co(TBP)-MOF	Lewis acid catalysis	Hydration of phenylacetylene	>99% (Yield)	-	[25]
Pt/PCN-224(Zn)	Oxidation catalysis	Alcohol oxidation reaction	>99%	>99%	[74]
Br-PCN-224(Fe)	Oxidation catalysis	Oxygenation of 3-methylpentane	99% (Yield)	>99%	[69]
ZJU-18	Oxidation catalysis	Oxidation of alkylbenzenes	>99%	>99%	[42]
PCN-602(Mn)	Oxidation catalysis	C-H bond halogenation	95% (Yield)	-	[43]
UNLPF-10	Photocatalysis	Photo-oxygenation of sulfides	>99%	-	[58]
PCN-222	Photocatalysis	Photoreduction of CO_2	-	30 μmol in 10 h for $HCOO^-$	[70]
MOF-525-Co	Photocatalysis	Photoreduction of CO_2	-	200.6 μmol $g^{-1}h^{-1}$ for CO 36.76 μmol $g^{-1}h^{-1}$ for CH_4	[76]
ZrPP-1-Co	Photocatalysis	Photoreduction of CO_2	-	14 μmol $g^{-1}h^{-1}$ for CO CO/CH_4 >96.4 %	[61]
TTCOF-Zn	Photocatalysis	Photoreduction of CO_2	-	12.33 μmol $g^{-1}h^{-1}$ for CO	[55]
Al-PMOF	Photocatalysis	Hydrogen evolution	-	200 μmol $g^{-1}h^{-1}$ for H_2	[28]
Por-sp^2c-COF	Photocatalysis	Oxidation of secondary amines	99% (Yield)	-	[54]
$Al_2(OH)_2$TCPP-Co	Electrocatalysis	Electrochemical reduction of CO_2	-	76% for CO TON = 1400	[71]
Hf_{12}-CoDBP	Electrocatalysis	Electrocatalytic proton reduction	-	TON = 32000 TOF = 17.7 s^{-1}	[22]
COF-367-Co (1%)	Electrocatalysis	Electrochemical reduction of CO_2	-	90% (Faraday efficiency) TON = 290000 TOF = 9400 h^{-1}	[45]
COF-366-Co	Electrocatalysis	Electrochemical reduction of CO_2	-	87% (Faraday efficiency)	[77]

Figure Captions.

Figure 1. Selected examples in the field of porphyrin framework compounds to date organized by the year in which they were first synthesized. Several significant discoveries in porphyrin MOFs (left) and COFs (right) are listed.

Figure 2. Examples of porphyrin building blocks used in porphyrin framework compounds. These include: 2,3,4, and 8-connected porphyrin linkers, functionalized and elongated porphyrin linkers used in MOFs, and 4-connected porphyrin monomers used in COFs.

Figure 3. Structures of porphyrin-based MOFs with varying inorganic building blocks. (A) MMPF-1(Cu) with $Cu_2(COO)_4$ clusters; (B) ZJU-18(Mn) with $Mn_2(COO)_4$ and $Mn_3(COO)_4(\mu_2\text{-}H_2O)_2$ clusters; (C) In-Co(TBP) with $In(COO)_4$ clusters; (D) Al-PMOF with $Al(\mu_2\text{-}OH)(COO)_2$ chains; (E) PCN-600(Fe) with $Fe_3(\mu_3\text{-}O)(COO)_6$ clusters; and (F) Zr-TCPP MOFs with $Zr_6(\mu_3\text{-}O)_4(\mu_3\text{-}OH)_4(COO)_n$ clusters including PCN-224, PCN-222/MOF-545, and MOF-525.

Figure 4. Catalytic applications of porphyrin framework compounds. (A) tandem catalysis; (B) oxidation catalysis; (C) photocatalysis; and (D-E) and electrocatalysis. (A) Adapted with permission from [68]; (B) adapted with permission from [69]; (C) adapted with permission from [70]; (D) adapted with permission from [45]; and (E) adapted with permission from [71].

Figures.

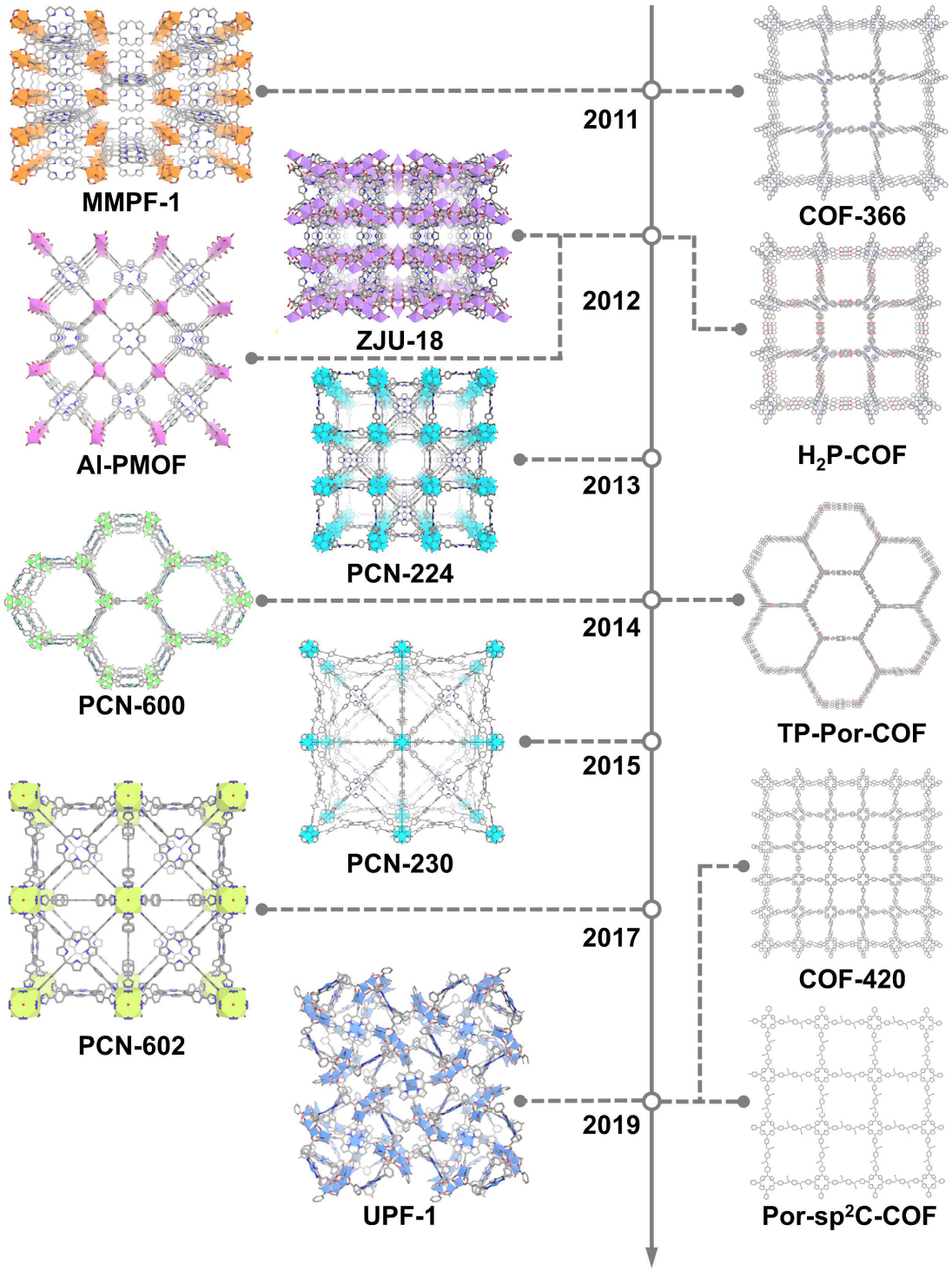

Figure 1.

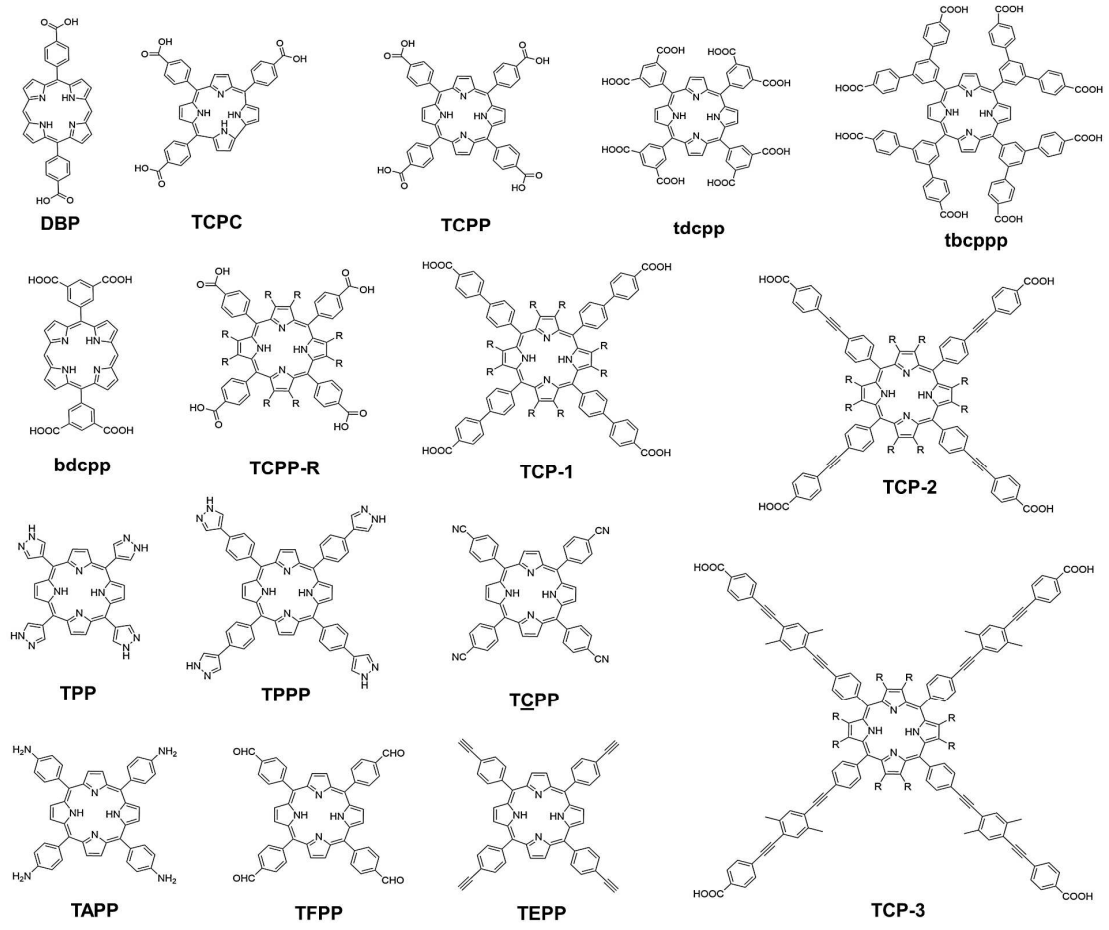
DBP
TCPC
TCPP
tdcpp
tbcppp
bdcpp
TCPP-R
TCP-1
TCP-2
TPP
TPPP
TCPP
TAPP
TFPP
TEPP
TCP-3

Figure 2.

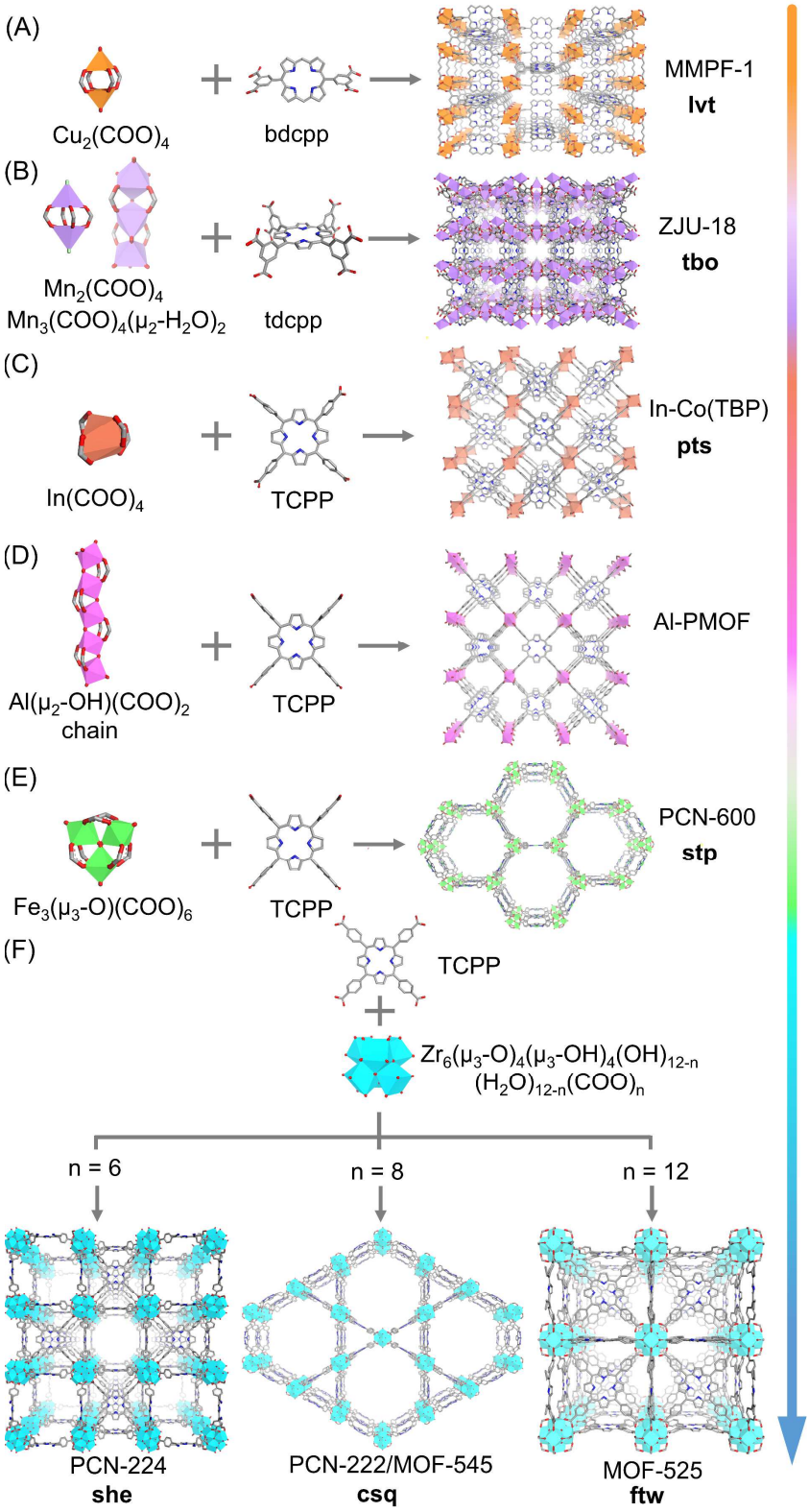
(A)
Cu2(COO)4
bdcpp
MMPF-1
lvt
(B)
Mn2(COO)4
Mn3(COO)4(μ2-H2O)2
tdcpp
ZJU-18
tbo
(C)
In(COO)4
TCPP
In-Co(TBP)
pts
(D)
Al(μ2-OH)(COO)2
chain
TCPP
Al-PMOF
(E)
Fe3(μ3-O)(COO)6
TCPP
PCN-600
stp
(F)
TCPP
Zr6(μ3-O)4(μ3-OH)4(OH)12-n
(H2O)12-n(COO)n
n = 6
n = 8
n = 12
PCN-224
she
PCN-222/MOF-545
csq
MOF-525
ftw

Figure 3.

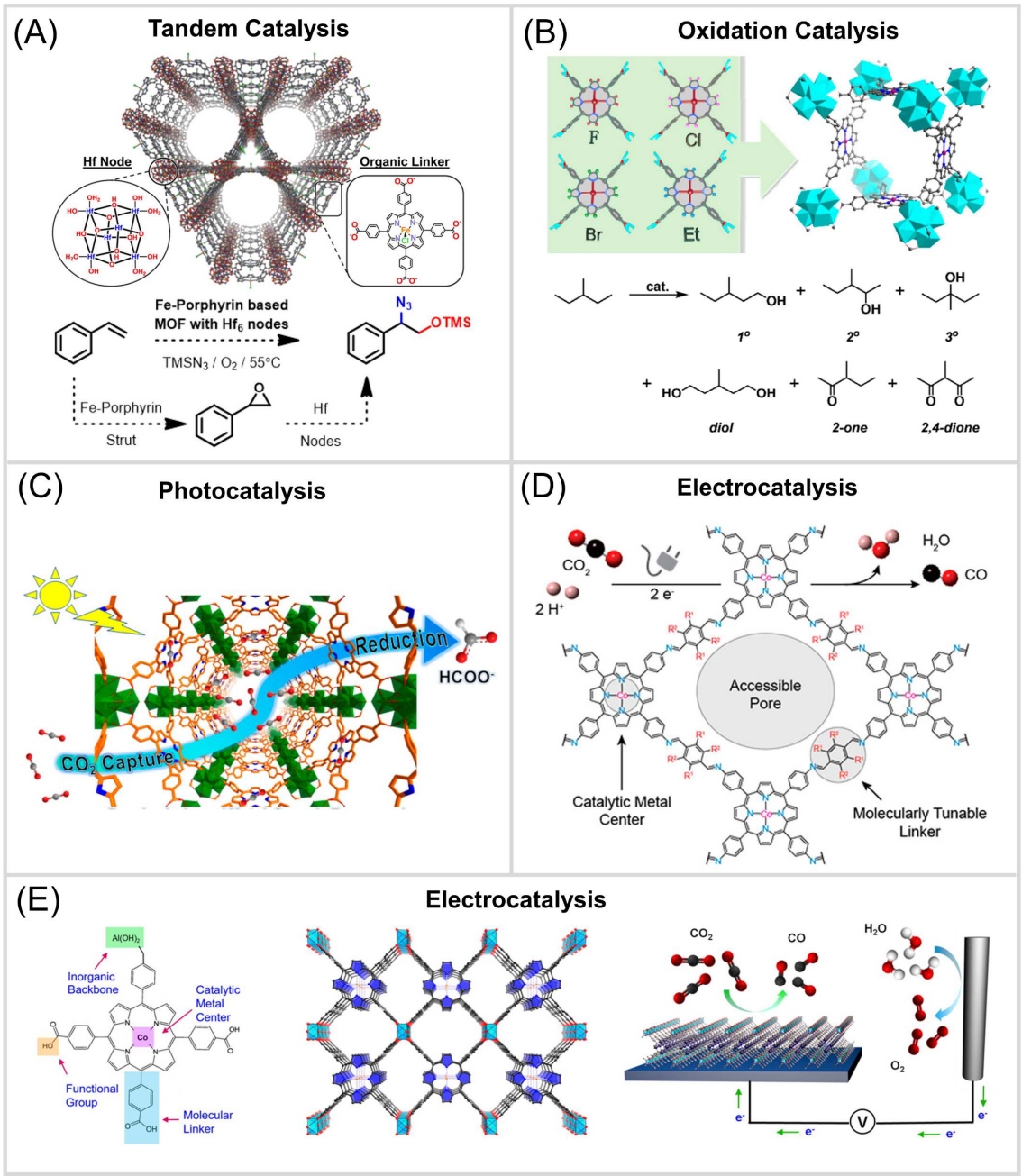
(A)
Tandem Catalysis
Hf Node
Organic Linker
Fe-Porphyrin based
MOF with Hf6 nodes
TMSN3 / O2 / 55°C
N3
OTMS
Fe-Porphyrin
Strut
Hf
Nodes
(B)
Oxidation Catalysis
F
Cl
Br
Et
cat.
OH
1°
2°
3°
HO
diol
2-one
2,4-dione
(C)
Photocatalysis
Reduction
HCOO-
CO2 Capture
(D)
Electrocatalysis
CO2
2 e-
2 H+
H2O
CO
Accessible
Pore
Catalytic Metal
Center
Molecularly Tunable
Linker
(E)
Electrocatalysis
Al(OH)2
Inorganic
Backbone
Catalytic
Metal
Center
Co
Functional
Group
Molecular
Linker
CO2
CO
H2O
O2
e-
V

Figure 4.